Multivariable control of 3D movement of an overhead crane with non-linear dynamics: Comparison between Pole-placement & MPC approaches

Mohammad Javad Hatami, * Hamed Moradi

Department of Mechanical Engineering, Sharif University of Technology, PO Box 11155-9567

Tehran, Iran, Tel: (+98) 21-66165545, Fax: (+98) 21-66000021

mj.hatami@mech.sharif.edu

** hamedmoradi@sharif.edu*

Abstract

Industrial workshops often require efficient overhead cranes, and a nonlinear system with four degrees of freedom is a standout choice. This system facilitates longitudinal and transverse movement of the crane trolley. However, the suspended load may experience disruptive vibrations in two directions. To address this, precise control is essential. This research focuses on developing two controllers: one based on pole-placement theory and another using a model predictive controller (MPC). Designing a pole-placement controller involves linearizing the system. Since the system is underactuated, two additional inputs are introduced, helping determine alternate poles with desired conditions. The pole-placement controller achieves rapid system response, exceeding input limits. The system modeled with the MPC controller exhibits a slower tracking process with a consistent 1^{o} vibration in the suspended load but stays within input limits. The response of each controller to uncertainties is compared. As a result, the pole-placement and MPC controllers create a robust system for specific regions and a system with variable vibration frequencies and low amplitudes, respectively. These controllers contribute to the efficient operation of overhead cranes in industrial workshops, ensuring both precise control and minimal load fluctuations.

Keywords: Overhead Crane, 3D Movement, Pole-Placement Controller, MPC Controller, Uncertainty.

1. Introduction

Overhead cranes consist of one or two parallel horizontal bridges that move within a specified range along warehouses or halls. These cranes play a vital role in material handling within industrial settings like warehouses, workshops, construction sites, and similar environments. The key control challenges for these cranes involve achieving rapid response and precision in reaching target locations, as well as quickly stabilizing the hanging load. In crane control, there are typically no direct forces applied to the load being moved by the crane. Moreover, overhead crane systems are inherently nonlinear and often exhibit various limitations, particularly in being underactuated. This means that the number of control inputs is fewer than the degrees of freedom, adding complexity to the control problem. These systems are susceptible to external disturbances, uncertainties, cable deflections, and may experience limitations in actuator force, further complicating the control task.

Early research on controlling overhead cranes involved the design of controllers using both open-loop and closed-loop circuit theories. Open-loop controllers operated without feedback, relying on the coordinated movement of the crane trolley and the hanging load to achieve desired trajectories and minimize fluctuations. Researchers like N. Sun et al. optimized control [1], L. Ramli et al. considered input shaping [2], and Z. Wu and X. Xia employed path modeling [3] to create controllers that effectively controlled load fluctuations and trajectory tracking. However, these open-loop controllers may struggle in the presence of disturbances and uncertainties. To address these challenges, more advanced open-loop controllers have been developed [4]. Nonetheless, the primary emphasis in crane control research remains on closed-loop controllers. Various methods have been explored in this category while adding different aspects of workspace limitations, including feedback control [5], energy-based control, such as energy coupling output feedback control for 4-DOF underactuated cranes [6], state-observer-based control [7], neural network approaches [8], adaptive control [9], sliding mode control (SMC) [10][11], combined adaptive sliding mode control with honey badger algorithm [12] where limitations are added by sorted databases, and even advanced variations like P-D sliding mode [13]. Many other controllers have also been developed within the framework of closed-loop feedback control.

In the context of overhead cranes, where disturbances and uncertainties are inherent, addressing instability challenges is crucial. Methods [10] and [13] have demonstrated their effectiveness due to the robustness but their approach does not seem to be flexible enough respecting the mass of the hanging load. Overhead cranes, being underactuated systems, pose inherent complexity. To tackle this, some approaches, like [13], linearize the system and employ P-D sliding mode control. Recent research has also utilized Lyapunov techniques and LaSalle's invariance principle to design stabilized underactuated control systems, as seen in [14] and [15], which also incorporate PID-coupling control. Additionally, fuzzy adaptive nonlinear controllers and optimal controllers have been employed, even for double pendulum cranes, which can be prone to instability in certain cases [16][17]. A multitude of methods and modern approaches, including passivity-based adaptive control [18] and combing it with online reinforcement learning for real-time control [19] and also sliding mode [20] for heavy and precise duties, are available in the field of overhead crane control.

Although various methods have shown promising results, recent approaches often focus on specific input amplitudes and short trajectory plans for simulations. Given that system behavior hinges on minimizing load fluctuations, it's crucial for the trolley to reach its target with minimal vibrations. The damping ratio and natural frequency of the system play pivotal roles in this regard. Pole-placement theory, known for its simplicity and stability, can be effective in achieving rapid responses. Meanwhile, the MPC controller is well-suited to operate within input force limitations and handle fluctuation amplitudes. Bao et al. used system's performance as feedback in an MPC algorithm for a 2D bridge crane as a proof of the usage of presented controller type in this area [21]. Recognizing these differences, this paper explores the use of both a pole-placement controller and an MPC controller to design a comprehensive solution that offers a wider range of desired inputs and rapid response capabilities. Further details on controller design, simulation, result comparisons, and testing under uncertain conditions will be discussed in subsequent sections.

In summary, in this context following details and reasons are explained:

- System mathematical model and considered transportation, its analysis and linearizing it by transforming it into a state-space model
- Designing controllers using pole-placement and model predictive approaches
- Simulation and closed-loop response analysis
- Comparison of system behavior with different controllers
- Final check and uncertainties analysis

2. System dynamics and its nonlinear characteristics

The dynamical model used in this study, as introduced in [13], is a state-of-the-art and comprehensive model that addresses fundamental issues. What sets this model apart from others is its three-dimensional nature. As illustrated in Figure 1, in an x-y-z coordinate system, a trolley is situated on a bridge capable of moving along its length (the y-axis), and the combination of the bridge and crane trolley can move along the x-axis. Additionally, a hanging load is attached to the trolley by a cable. For simplicity in calculations, the weight of the cable is disregarded.

The trolley is positioned on a bridge, where F_x represents the input force to move the entire system along the x-axis, dragging the bridge and its contents. F_y is another input force used to transport the trolley along the y-axis. The load is suspended from the trolley by a rigid, constant-length cable, resulting in fluctuations that manifest as angular deflections, θ_x and θ_y.

The primary system comprises two inputs and four outputs, suggesting the possibility of it being an underactuated plant. To address this, additional inputs can be introduced to apply torque to the hanging load, reducing its oscillations. Employing the Lagrange method and simplifying the results using MATLAB, considering the system's four degrees of freedom, the dynamic equations are derived as follows:

$$\left(M_x + m_p\right)\ddot{x} + m_p l\ddot{\theta}_x C_x C_y - m_p l\ddot{\theta}_y S_x S_y - 2m_p l\dot{\theta}_x\dot{\theta}_y C_x S_y - m_p l\dot{\theta}_x^2 S_x C_y - m_p l\dot{\theta}_y^2 S_x C_y = F_x - f_{rx} \quad (1)$$

$$\left(M_y + m_p\right)\ddot{y} - m_p l\ddot{\theta}_y C_y + m_p l\dot{\theta}_y^2 S_y = F_y - f_{ry} \quad (2)$$

$$m_p l\ddot{x} C_x C_y + m_p l^2\ddot{\theta}_x C_y^2 - 2m_p l^2\dot{\theta}_x\dot{\theta}_y C_y S_y + m_p g l S_x C_y = 0 \quad (3)$$

$$-m_p l\ddot{x} S_x S_y - m_p l\ddot{y} C_y + m_p l^2\ddot{\theta}_y + m_p l^2\dot{\theta}_x^2 C_y S_y + m_p g l C_x S_y = 0 \quad (4)$$

where, M_x stands for the trolley mass, M_y for the trolley mass and the bridge mass together, m_p for the payload mass, l for the length of the cable, and g represents the gravity coefficient. S_y, S_x, C_y and C_x, are brief words to describe $\sin\theta_y$, $\sin\theta_x$, $\cos\theta_y$ and $\cos\theta_x$ respectively. Also, f_{rx} and f_{ry} are friction coefficients through x and y directions. According to [22], these coefficients are usually a mixture of hyperbolic and polynomial functions. Therefore, in this case, friction has equations like these:

$$f_{rx} = f_{rox}\tanh\left(\frac{\dot{x}}{\varepsilon_x}\right) - k_{rx}\left|\dot{x}\right|\dot{x} \quad (5)$$

$$f_{ry} = f_{roy}\tanh\left(\frac{\dot{y}}{\varepsilon_y}\right) - k_{ry}\left|\dot{y}\right|\dot{y} \quad (6)$$

The coefficients in the equations above represent friction-related factors, and their values have been determined through experimental means.

3. Linearized dynamic system and its State Space configuration

In the case of underactuated systems, dealing with a nonlinear system presents a significant challenge as achieving desired functional results can be problematic when the system lacks full controllability. Additionally, working with a nonlinear system can introduce complexities into the process. Therefore, to enhance the performance when designing a pole-placement controller, which relies on precise system state-space matrices, it is essential to employ a linearized model.

The industrial example simulated in this paper is based on the overhead crane system introduced in [13]. To facilitate a more convenient comparison between controllers, the same parameter values as those introduced in [13] are used. Consequently, M_x and M_y are set to 6.157 kg and 15.594 kg, respectively. The mass of the hanging load, m_p, is considered as 1 kg, while the length of the cable l, with its neglected mass, is set at 0.6 m. The gravity coefficient is assumed to be 9.8 m/s^2. Finally, for equations 5 and 6, the friction coefficients and their respective values are as follows:

$$f_{rox} = 23.652(N),\ f_{roy} = 20.371(N), \varepsilon_x = \varepsilon_y = 0.01, k_{rx} = -0.8, k_{ry} = -1.4 \qquad (7)$$

To utilize gathered equations in an actual industrial instance, the work requires a linearized system. So, equations 1 to 4 can be directly linearized while being transformed into state-space matrices. Therefore, linearization of the system is completed by Jacobian matrices and using MATLAB according to the nonlinear system around the operating point. The obvious thing is the fact that the final derivatives of state-space variables are $\ddot{x}$, $\ddot{y}$, $\ddot{\theta}_x$ and $\ddot{\theta}_y$. Thus, the equations 1 to 4 are divided concerning the final derivatives of the variables where they also contain lines of the derivatives of the state variables and shown by f_i where i can be number one to four; furthermore, x_n is assigned to the variables where n is the number of variables which is set to be 8 due to system information. Similarly for outputs, g_j is assigned where j can be any number from 1 to four and at last, for inputs u_k stands for the system force entries where k has to be one or two. Now, to linearize the system and achieve a state-space model, there are no operating points for x and y, and other parameters are linearized around the zero-operating point. Due to all the explanations, according to equation 8, state-space matrices are completely generated.

$$A = \left.\frac{\partial \mathbf{f}}{\partial \mathbf{x}}\right|_{(\mathbf{x}_0,\mathbf{u}_0)} = \begin{bmatrix} \left.\frac{\partial f_1}{\partial x_1}\right|_{(\mathbf{x}_0,\mathbf{u}_0)} & \cdots & \left.\frac{\partial f_1}{\partial x_n}\right|_{(\mathbf{x}_0,\mathbf{u}_0)} \\ \vdots & \ddots & \vdots \\ \left.\frac{\partial f_n}{\partial x_1}\right|_{(\mathbf{x}_0,\mathbf{u}_0)} & \cdots & \left.\frac{\partial f_n}{\partial x_n}\right|_{(\mathbf{x}_0,\mathbf{u}_0)} \end{bmatrix}, B = \left.\frac{\partial \mathbf{f}}{\partial \mathbf{u}}\right|_{(\mathbf{x}_0,\mathbf{u}_0)} = \begin{bmatrix} \left.\frac{\partial f_1}{\partial u_1}\right|_{(\mathbf{x}_0,\mathbf{u}_0)} & \cdots & \left.\frac{\partial f_1}{\partial u_n}\right|_{(\mathbf{x}_0,\mathbf{u}_0)} \\ \vdots & \ddots & \vdots \\ \left.\frac{\partial f_n}{\partial u_1}\right|_{(\mathbf{x}_0,\mathbf{u}_0)} & \cdots & \left.\frac{\partial f_n}{\partial u_n}\right|_{(\mathbf{x}_0,\mathbf{u}_0)} \end{bmatrix}$$

$$C = \left.\frac{\partial \mathbf{g}}{\partial \mathbf{x}}\right|_{(\mathbf{x}_0,\mathbf{u}_0)} = \begin{bmatrix} \left.\frac{\partial g_1}{\partial x_1}\right|_{(\mathbf{x}_0,\mathbf{u}_0)} & \cdots & \left.\frac{\partial g_1}{\partial x_n}\right|_{(\mathbf{x}_0,\mathbf{u}_0)} \\ \vdots & \ddots & \vdots \\ \left.\frac{\partial g_n}{\partial x_1}\right|_{(\mathbf{x}_0,\mathbf{u}_0)} & \cdots & \left.\frac{\partial g_n}{\partial x_n}\right|_{(\mathbf{x}_0,\mathbf{u}_0)} \end{bmatrix}, D = \left.\frac{\partial \mathbf{g}}{\partial \mathbf{u}}\right|_{(\mathbf{x}_0,\mathbf{u}_0)} = \begin{bmatrix} \left.\frac{\partial g_1}{\partial u_1}\right|_{(\mathbf{x}_0,\mathbf{u}_0)} & \cdots & \left.\frac{\partial g_1}{\partial u_n}\right|_{(\mathbf{x}_0,\mathbf{u}_0)} \\ \vdots & \ddots & \vdots \\ \left.\frac{\partial g_n}{\partial u_1}\right|_{(\mathbf{x}_0,\mathbf{u}_0)} & \cdots & \left.\frac{\partial g_n}{\partial u_n}\right|_{(\mathbf{x}_0,\mathbf{u}_0)} \end{bmatrix} \qquad (8)$$

To clarify, the approach employed here is akin to using partial differential methods for linearization, which yields a linearized state-space model around the chosen operating points. These linearized matrices serve as the foundation for designing both pole-placement and MPC controllers. With the state-space model in hand, determining the controllability matrices becomes a straightforward process. Following the acquisition of state matrices, controllability matrices are computed, setting the stage for controller design under various conditions. The state-space matrices are detailed in equation 9.

$$A_{8\times 8}=\begin{bmatrix}0&1&0&0&0&0&0&0\\0&-384.15&0&0&1.59&0&0&0\\0&0&0&1&0&0&0&0\\0&0&0&-130.63&0&0&-0.63&0\\0&0&0&0&0&1&0&0\\0&640.25&0&0&-18.99&0&0&0\\0&0&0&0&0&0&0&1\\0&0&0&-217.72&0&0&-17.38&0\end{bmatrix},B_{8\times 2}=\begin{bmatrix}0&0\\0.16&0\\0&0\\0&0.06\\0&0\\-0.27&0\\0&0\\0&0.11\end{bmatrix} \quad (9)$$

$$C_{4\times 8}=\begin{bmatrix}1&0&0&0&0&0&0&0\\0&0&1&0&0&0&0&0\\0&0&0&0&1&0&0&0\\0&0&0&0&0&0&1&0\end{bmatrix},D_{4\times 2}=\begin{bmatrix}1&0\\0&0\\0&0\\0&0\end{bmatrix}$$

4. Design of Pole-Placement and MPC controllers

4.1. Pole-Placement Controller Design

An intelligent system consists of three core components: a sensor, a controller, and an actuator. The sensor observes and measures system responses, which are then compared to the desired input by the controller. Based on this comparison, the controller generates appropriate commands for the actuator to achieve the desired outcome.

The primary objective of designing a controller using the pole-placement method is to manipulate the locations of each pole, thereby ensuring that the system responses align with the desired conditions. To begin this process, the controllability of the system is assessed using the matrices in equation 9. The controllability matrix takes the form:

$$S=\begin{bmatrix}B & AB & A^2B\ldots & A^{n-1}B\end{bmatrix} \quad (10)$$

In a fully controllable system, the rank of the S matrix must match the number of state variables. In essence, a system achieves full controllability when its controllability matrix is invertible. As previously demonstrated, the system encompasses 8 state variables, thus confirming controllability through the application of equation 10.

$$S=\begin{bmatrix}B, AB, A^2B, A^3B, A^4B, A^5B, A^6B, A^7B\end{bmatrix} \quad (11)$$

After calculating equation 11, it becomes evident that the system has a rank of 2, indicating a substantial disparity between the system's rank and the number of state variables. In essence, only two of the system's parameters are controllable.

To address this challenge, two approaches can be considered. Firstly, the system can be partitioned into controllable and uncontrollable parts, and a controller designed specifically for the controllable portion. Utilizing mappings and transfer matrices, it might be possible to control all eight variables. However, it's crucial to verify the stability of the resulting poles in this approach.

Alternatively, when the rank is notably low, an alternative solution is to introduce additional inputs to the primary system until it attains full rank, effectively creating a new system. The stability of this control system should be rigorously assessed each time additional inputs are added, as this may pose a threat. Subsequently, by matching the poles of the alternative system with those of the primary system, the results can be evaluated. If the response is satisfactory, this adapted approach can often be more straightforward and accessible than the first one. In this paper, the second option is employed and successfully implemented.

To put the last paragraph in other words, two more actuators are set on the trolley, and their mass is neglected to control the fluctuation of the hanging load. As a result, they have minor effects on friction which can be ignored. To change the main system to an alternate one, torque inputs T_x and T_y are added at the right side of equations 3 and 4. Considering these changes, matrix A from equation 9 will stay constant. Still, dimensions of matrix B will increase to be four columns as the additional two actuators. Following the application, two zero columns are added to the transfer matrix D. Thus, the input matrix will be like below:

$$B = \begin{bmatrix} 0 & 0 & 0 & 0 \\ 0.16 & 0 & -0.27 & 0 \\ 0 & 0 & 0 & 0 \\ 0 & 0.06 & 0 & 0.11 \\ 0 & 0 & 0 & 0 \\ -0.27 & 0 & 3.23 & 0 \\ 0 & 0 & 0 & 0 \\ 0 & 0.11 & 0 & 2.95 \end{bmatrix} \tag{12}$$

As explained before, controllability should be checked one more time. By manipulating a generalized equation in equation 10 for systems with multiple entries, equation 13 is gained.

$$S = \left[B \;\; AB \;\; A^2B \ldots \;\; A^{n-m}B \right] \tag{13}$$

where m is the number of system inputs, this matrix equates to equation 10 and is a faster way for reaching the answer. Therefore, for the alternate system with four entries it is obtained that:

$$S = \left[B, AB, A^2B, A^3B, A^4B \right] \tag{14}$$

In equation 14, the controllability matrix is found to be full rank, confirming the full controllability of the alternate system as expected through the addition of new inputs. This result indicates that by selecting and replacing the appropriate poles, the control system can be successfully established for the alternate system.

In the case of an overhead crane system with a hanging load, optimal performance is achieved when the trolley and the bridge smoothly reach the desired destination without excessive speed, resulting in a lower settling time. This is particularly crucial when the travel distance exceeds approximately 1 meter. High-speed trolley movement can lead to significant vibrations in the hanging load, potentially pushing the system out of desirable conditions. This is because the cable and rod connecting the trolley to the hanging load in the actual model are not rigid bodies, emphasizing the importance of maintaining a small angle.

To initiate the process, the system's poles must be determined. Using matrix A from equation 9, the poles of the system are extracted. Notably, matrix A remains constant in both the main and alternate systems.

$$poles = \left[0, 0, -384.14, -0.003 \pm 4.04j, -130, -0.004 \pm 4.04j \right] \tag{15}$$

The distance between a pole and the imaginary axis in pole placement dictates its influence on the system's performance. The system's behavior is primarily determined by its dominant poles. To optimize performance, the approach is to position six poles close to the imaginary axis to achieve a faster response without imposing high input forces. The remaining two poles are designated as the dominant poles.

Concerning these facts, settling time can be assumed around 10 seconds, which can be sufficient, and for maximum overshoot, roughly 3% can be a good value. By these conditions, dominant poles are calculated, and to reduce the effects of the other poles, they should be set far away from the imaginary axis. Using equations for maximum overshoot and settling time, the natural frequency ω_n and the damping ratio ζ of the desired system are found as:

$$M = e^{-\frac{\zeta\pi}{\sqrt{1-\zeta^2}}} \rightarrow \zeta \cong 0.745 \tag{16}$$

$$t_s = \frac{4}{\zeta\omega_n} \rightarrow \omega_n = 0.537\frac{rad}{s} \tag{17}$$

Thus, the achieved desired poles are:

$$p_{1,2} = \omega_n\left(-\zeta \pm \sqrt{1-\zeta^2}\right) \rightarrow p_{1,2} = -0.4 \pm 0.3584j \tag{18}$$

$$p_3 = -5, p_4 = -6, p_5 = -7, p_6 = -8, p_7 = -9, p_8 = -10 \tag{19}$$

So that the gain matrix K shown below is pulled out for the alternate system with four actuators and ready to be manipulated.

$$K_{4\times8} = \begin{bmatrix} 82 & 2291.7 & 119.6 & 14.4 & -120.7 & -7.5 & 0 & 0 \\ 382.4 & 46.2 & 744.4 & -1808.2 & -355.7 & -47.6 & -18.2 & -6.6 \\ 3.3 & 5.8 & 2.3 & 0.2 & -10.1 & 2.7 & 0 & 0 \\ -13.8 & -1.7 & -26.9 & -8.3 & 12.9 & 1.7 & 4.9 & 4.0 \end{bmatrix} \tag{20}$$

To evaluate the performance of the achieved gain, regulation responses for K are examined. Initial values are assigned to each state variable, and a regulation diagram is generated by solving the differential equation. This process serves as a test of the controller's effectiveness. In the context of pole-placement theory:

$$u = -Kx \tag{21}$$

Here, u represents the problem inputs, while x denotes the state variables accessible through the state estimator. As illustrated in Figure 2, the regulation responses for each state variable demonstrate a clear and stable behavior, with reasonable maximum overshoots given the initial conditions. With this favorable system behavior confirmed, these poles can be tested in the main system. Utilizing the two inputs and the B matrix in equation 12, the controller gain is determined as per equation 22.

$$K_{2\times8} = \begin{bmatrix} 50.3 & -2210.7 & -3.3 & -29.4 & -494.4 & 11.1 & -75.1 & 12.5 \\ -911.1 & -449.2 & 372.4 & -1489.5 & 145.9 & -234.5 & 1402.9 & -106.6 \end{bmatrix} \tag{22}$$

By using equation 21 and solving the regulation equations once again, but with the main system dynamics, and using gain in equation 22, according to equation 23 with different initial values, Fig 3 is obtained.

$$\begin{cases} \dot{x} = Ax + Bu \\ u = -kx \end{cases} \tag{23}$$

As depicted in Figure 3, the system variables converge to zero from their initial conditions at an appropriate pace, with the error stabilizing at zero. It's evident that the replaced poles from the alternate system not only perform exceptionally well in the main system but also result in lower maximum overshoot factors for specific variables. Consequently, the pole-placement controller is designed using the obtained gain from equation 22 and subsequently applied in the simulation.

4.2. Model Predictive Controller (MPC) Design

Model Predictive Control (MPC) is a powerful strategy for Multi-Input Multi-Output (MIMO) systems, known for its ability to provide precise control while accommodating various constraints. This method involves optimizing the controller's actions over a set horizon to minimize a cost function, gradually reducing the error to zero.

In essence, MPC is rooted in optimal control principles. It predicts the system's future behavior and then selects the most desirable inputs to achieve optimal control. However, MPC relies on the system's initial states, as reflected in the state-space model equations detailed in equation 9. These equations provide a linear, time-varying model with matrices for use in MPC.

$$\begin{aligned}&\frac{dx}{dt}=A(t)x+B(t)u\\&y=C(t)x+D(t)u\\&x(0)=x_0\end{aligned}\tag{24}$$

When discussing MPC controllers, it's often more convenient to work with a discrete-time model. This approach yields a linear, time-invariant, and discrete-time model that aligns better with the MPC framework.

$$\begin{aligned}&x(k+1)=Ax(k)+Bu(k)\\&y(k)=Cx(k)+Du(k)\\&x(0)=x_0\end{aligned}\tag{25}$$

The linear discrete-time model is preferable for explaining MPC concepts simply and effectively. One of the notable advantages of MPC is its ability to manage constraints and keep the system within predefined limits. The inputs in the system have bounds, and MPC is adept at handling these constraints.

$$\begin{aligned}&Eu(k)\le e \qquad k\in\mathbb{Z}\ge 0\\&E=\begin{bmatrix}I\\-I\end{bmatrix}\quad e=\begin{bmatrix}\max(u)\\-\min(u)\end{bmatrix}\end{aligned}\tag{26}$$

States are not exempt from these constraints, so when the need arises to control and manage the states, the boundaries are defined as:

$$Fx(k)\le f \qquad k\in\mathbb{Z}\ge 0\tag{27}$$

F and f processes like E and e, respectively [23]. In a time-varying system, the linear quadratic regulator or LQR is given as a cost function [24][25].

$$J=\frac{1}{2}\int_0^T\left(x^TQx+u^TRu\right)dt+\frac{1}{2}x^T(T)Px(T)$$

in which $Q\ge 0$, $R>0$, $P\ge 0$ are positive, symmetric definite matrices. In MPC controller, since the discrete-time model is used, this cost function is transformed to a summing equation as:

$$J(x_0,u)=\frac{1}{2}\sum_{k=0}^{N-1}\left(x^T(k)Qx(k)+u^T(k)Ru(k)\right)+\frac{1}{2}x^T(N)Px(N)\tag{28}$$

In the formula above, N represents the number of time steps into the future considered. Symmetry matrices are selected to be diagonal, indicating the weight of each parameter. The controller's objective is to use collected data to predict the system's behavior by minimizing the cost function and driving u to converge to zero.

Choosing the optimal LQR weights can be done in various ways [24], but in this study, effective parameters are set using software tools, allowing for an automated process.

The sample time, denoted as T_s is a critical factor in controller design. Longer sample times introduce more uncertainties and disturbances with delayed reactions, while shorter sample times result in a faster system but increase error comparisons. Given the system's pole locations and the need for performance, the sample time cannot be less than 1 second, and, in this case, T_s is set to 1 second.

The prediction horizon p, determines how far into the future the controller predicts the system's behavior. Choosing p too small leads to wasted time due to delays and prolonged settling times, while a too-large p amplifies the impact of uncertainties and disturbances. To optimize performance, equation 29 is used to select a suitable p, ensuring that the system exhibits desirable behavior.

$$p.T_s\ge t_s\tag{29}$$

The settling time, denoted as t_s, is set to 10 seconds, consistent with previous parts, while T_s remains at 1 second. This configuration results in a prediction horizon p equal to or greater than ten seconds, and thus p is set to 10 seconds in subsequent calculations.

Moving forward, the control horizon m is the next factor to consider, primarily aimed at reducing error comparisons. Consequently, it should not fall below a certain limit. Similar to determining the prediction horizon, m can be calculated using equation 30:

$$0.1p \le m \le 0.2p \tag{30}$$

while having p on 10 seconds, m is considered on 1 second.

The next step involves setting constraints and weights for the system parameters, a notable feature of the MPC controller. Depending on the situation, MPC can accommodate two types of constraints: soft and hard. In this specific problem, hard constraints are preferred for the system inputs, limiting them to 400 N. This constraint is chosen to prevent excessive trolley speed, which could lead to increased fluctuations in the hanging load. Additionally, constraints are imposed on the vibration amplitude, restricting it to no more than 2 degrees in both directions, disregarding air drag forces. As a result, the system is expected to respond cautiously rather than rapidly, given the constraints placed on input forces.

In a similar vein, when determining the weights, it's essential to consider that using the full control power to manage vibrations may not be ideal. Given the greater weight of the trolley and its impact on angles, excessively sensitive control may not yield better performance. In this particular problem, the primary emphasis is on achieving the system's appropriate behavior, with the approach being either aggressive or robust.

Moreover, it's evident that enhancing robustness may result in higher input forces, which is not desirable in this specific industrial context. Therefore, the controller parameters, as detailed in Table 1, are configured to prioritize the system's suitable performance. Subsequent to simulation, further adjustments can be made to fine-tune the controller, depending on the specific conditions and environment in which the machine will operate.

5. Simulation, system response analysis & discussion

This section aims to simulate the system using both controllers and analyze their responses. The desired performance criteria are achieving speed while mitigating fluctuations resulting from trolley movement.

5.1. System Simulation with Controller Designed by Pole-Placement Method

A system equipped with a pole-placement controller is represented by a schematic block diagram in Fig 4. Here, r denotes the desired input, and x represents the system's state variables. The desired destination is set at point (3,4) meters on the Cartesian coordinates for the main system. By conducting simulations using the controller design's K value, the system's responses are depicted in Fig 5.

In Fig 5a, the system response exhibits a slight maximum overshoot, which is deemed adequate. The response achieves a smooth and desirable pace in reaching the destination, with a settling time of approximately 10 seconds, aligning with expectations. In Fig 5b, although the response initially exhibits rapid fluctuations, the amplitude reaches 10 degrees at the outset but quickly stabilizes around the equilibrium point. This behavior was anticipated, as the system prioritizes rapid destination attainment, as evident from Fig 5a.

Subsequently, the input forces are examined, as displayed in Fig 6. Notably, the force reaches approximately 2200 N, which is consistent with operational conditions and is deemed reasonable but not optimized. The majority of this input force is allocated to achieving movement speed and promptly mitigating vibrations, as anticipated in the response. These results are obtained when the system is required to reach a destination exceeding one meter.

The simulation is set similarly to track the point (0.3,0.4) meters for minor transportation like less than one meter and gathered diagrams are set in Figs 7 and 8. It can even be helpful to compare the results to the one gained in [13]. This should be noted that in previous sections the settling time is set for 10 seconds which is higher than [13] so the system comprises better damping on fluctuations and more than 1 meter destinations.

In Fig 7a, the settling time remains consistent with the previous simulation. Consequently, the system response is slower than in Fig 6a. Fig 7b demonstrates that the system's fluctuations are effectively damped and do not exceed 1 degree. This design proves to be highly responsive for transportations less than one meter.

Changes in the input force are presented in Fig 8. Notably, the input force experiences a significant decrease, falling below 220 N. This reduction is attributed to the shorter travel distance, allowing the system to operate at a smoother and slower pace without saturating the actuator.

5.2. System Simulation with Controller Designed by MPC approach

Similar to subsection 5.1, the system block diagram is configured as shown in Fig 9. The state estimator feeds the variables into the controller, and the MPC theory focuses on minimizing the cost function. It achieves this by predicting the system's behavior within the specified prediction horizon and subsequently transmitting the control signal to the trolley and crane system.

During the simulation, Table 1 is configured for the MPC controller plant, while all other factors are automatically generated. Once the simulation is complete, the responses for the desired (3,4) meters location are presented in Fig 10.

In Fig 10a, the system takes approximately 30 seconds to reach its desired location, which is longer than our specified settling time. Notably, there is no maximum overshoot, and the system exhibits overdamped behavior. Fig 10b illustrates that the system experiences steady-state vibrations with a 2-degree amplitude after approximately 20 seconds, as expected. These vibrations should ideally be damped by friction from air drag force, which was not accounted for in our model. Finally, Fig 10c presents the input forces.

Due to the constraint on input force set at 400 N, the actuator force remains within limits for a sample time of 1 second, demonstrating the system's response. These outcomes are observed when the desired input movement exceeds 1 meter. To facilitate comparison, the analysis is repeated for a target point of (0.3,0.4) meters, mirroring section 5.1. The results are depicted in Fig 11.

In Fig 11a, the settling time is under 30 seconds, with no maximum overshoot observed. Compared to Fig 10b, the system exhibits a slower response. As a result, Fig 11b shows fluctuations not surpassing 1 degree, indicating that this controller effectively mitigates vibrations for shorter destinations. Changes in input force are illustrated in Fig 11c. Here, the input force remains below 120 N, adhering closely to its constraints. An increase in this factor enhances system speed, leading to greater amplitudes in hanging load vibrations.

6. Comparison of the performance of designed controllers

In the previous sections, we designed different controllers using pole-placement and MPC approaches, observing their distinct responses when applied to the system. These results exhibit variations, with each controller having specific conditions for optimal use. Consequently, it's essential to compare these designed controllers and elucidate their operational characteristics. Furthermore, we outline the differences between our controllers and the PD-SMC controller from [13].

The simulation results reveal that the movement of the trolley in Cartesian coordinates yields diverse responses and behaviors, not only across different controllers but also in scenarios involving short or long distances. Plots are provided in Figs 12 and 13 to illustrate these outcomes.

In Fig 12a, it's evident that for distances less than one meter, the pole-placement controller exhibits slightly higher speed compared to the MPC controller. However, the MPC controller, represented by the dotted lines, showcases smoother movement without overshoot, even when the maximum overshoot for the pole-placement controller remains below 3%.

Regarding oscillations, Figs 12b and 12c demonstrate that the pole-placement controller leads to quicker convergence to zero and equilibrium point, while the MPC controller allows for vibrations of approximately 1 degree. This minimal angle is acceptable, especially in scenarios with longer cables between the load and trolley. The MPC controller dampens vibrations at a slower rate than the pole-placement controller, but eventually reaches a zero equilibrium point, which simulates the presence of drag force in real-world situations. In terms of input forces, Fig 13 reveals that the MPC controller applies lower input force to the system compared to the pole-placement controller, which uses about twice the force.

In summary, for distances less than one meter, the choice between controllers depends on system speed and the need to quickly dampen fluctuations. The pole-placement controller excels in these conditions, provided the actuator can deliver the necessary force. However, if there's a force input limit and overdamping is desirable, the MPC controller is a cost-effective option.

Comparing to [13], the PD-SMC controller performs well, with even lower input force as shown in Fig 13. However, this performance is primarily optimized for distances less than one meter. When distances increase to around 4 meters, the system experiences more vibrations and approaches the limit of desired performance. Moving forward, the focus shifts to comparing controller behaviors when moving the trolley to a long-distance point like (3,4) meters, and evaluating which one performs better in different conditions in Figs 14 and 15.

In Fig 14a, the differences between both systems are evident, with the pole-placement controller maintaining a consistent settling time of 10 seconds. Similar to Fig 12a, the MPC controller displays a smoother behavior but at a slower speed compared to the pole-placement controller. This reduced speed keeps the fluctuation amplitudes shown in Figs 14b and 14c within the constraints of 2 degrees in a steady-state condition.

For the pole-placement controller, however, there is an initial deviation of 10 degrees from the equilibrium point, which is expected due to its high speed. This is not a desirable performance, but it is quickly damped and doesn't persist like in the MPC controller.

Regarding input forces, the MPC controller doesn't exceed the 400 N saturation limit set for the actuator. In contrast, the pole-placement controller applies a significant input force to the system. Therefore, the pole-placement controller designed without input force limits performs exceptionally well and handles the 10-degree deflection without issue. It is also suitable when a fast system is needed, especially for distances greater than one meter.

On the other hand, the MPC controller provides smoother movement while adhering to input force constraints, making it a favorable choice when overshoots are to be avoided in a scenario with limitations on input forces.

7. Analyzing the control system behavior in the presence of uncertainties

In this section, a brief analysis of the control system's robustness is conducted. Real-world systems are subject to changing conditions over time, and a controller must be able to adapt to these variations. For example, in our scenario, parameters like the mass of the hanging load, trolley mass, and cable length can change over time, affecting the system's behavior. To evaluate the robustness of our controllers, we introduce 10% uncertainties by either adding or subtracting this percentage from each of these parameters. The results of this robustness analysis are as follows:

$$\begin{cases} M_x' = M_x - \Delta M_x = 0.9 M_x = 5.54\,kg \\ m_p' = m_p + \Delta m_p = 1.1 m_p = 1.1\,kg \\ l' = l - \Delta l = 1.1 l = 0.66\,m \end{cases} \tag{31}$$

In this robustness analysis, both controllers, the pole-placement controller and the MPC controller, were subjected to variations in system parameters. The simulations showed that both controllers exhibited suitable robustness, with minimal sensitivity to changes in the system parameters related to the trolley's movement to reach the desired point, as depicted in Fig 16.

However, when it came to the fluctuations of the hanging load, the pole-placement controller displayed a more robust performance in the presence of uncertainties, as evident in Figs 17 and 18. The MPC-controlled system exhibited different responses with varying frequencies over time when uncertainties were introduced.

This analysis suggests that the pole-placement controller may offer better robustness in scenarios involving hanging load fluctuations. Further research in this field may yield additional insights into the sensitivity and robustness of different control systems for overhead cranes, as these systems continue to receive attention in the academic world.

8. Conclusions

In conclusion, this paper has explored the control of an overhead crane with four degrees of freedom and nonlinear dynamics, presenting various controller designs and their associated behaviors. Specifically, the pole-placement and MPC controllers were designed and simulated under realistic operational conditions. The pole-placement controller, designed for the underactuated system, employed two alternate inputs to simplify gain measurement. This controller exhibited excellent performance for both short and long-distance movements, although its high-speed operation led to increased vibrations in the hanging load. While it occasionally required high input forces, it demonstrated robustness in damping uncertainties.

Conversely, the MPC controller, which minimizes a cost function based on system parameters, provided smoother and slower system responses with reduced hanging load fluctuations. It effectively constrained input forces, ensuring system performance met the constraints in both movement and oscillations. The choice between controllers depends on the specific application and operational requirements.

In summary, as demonstrated in Table 2, each controller offers distinct advantages, making them suitable for different scenarios. The process under uncertainty involvement conditions should be considered as well. The selection of the appropriate controller should be based on the specific needs and conditions of the system's operation.

9. Declarations

- Funding: Not applicable. No funding.
- Conflict of Interest: Non declared.

References

[1] Sun, N., Wu, Y., Chen, H., et al. "An energy-optimal solution for transportation control of cranes with double pendulum dynamics: Design and experiments", *Mechanical Systems and Signal Processing* 102, pp. 87-101. (2018)

[2] Ramli, L., Mohamed, Z. and Jaafar, H. I. "A neural network-based input shaping for swing suppression of an overhead crane under payload hoisting and mass variations", *Mechanical Systems and Signal Processing* 107, pp. 484-501. (2018)

[3] Wu, Z. and Xia, X. "Optimal motion planning for overhead cranes", *IET Control Theory & Applications* 8(17), pp. 1833-1842. (2014)

[4] Fujioka, D. and Singhose, W. "Optimized input-shaped model reference control on double-pendulum system", *Journal of Dynamic Systems, Measurement, and Control* 140(10), pp. 101004. (2018)

[5] Chang, C.Y. and Lie, H.W. "Real-time visual tracking and measurement to control fast dynamics of overhead cranes", *IEEE Transactions on Industrial Electronics* 59(3), pp.1640-1649. (2011)

[6] Sun, N., Fang, Y. and Zhang, X. "Energy coupling output feedback control of 4-DOF underactuated cranes with saturated inputs", *Automatica* 49(5), pp. 1318-1325. (2013)
[7] Chen, W. and Saif, M. "Output feedback controller design for a class of MIMO nonlinear systems using high-order sliding-mode differentiators with application to a laboratory 3-D crane", *IEEE Transactions on Industrial Electronics* 55(11), pp. 3985-3997. (2008)
[8] Cuong, H.M., Van Trieu, P., Nho, L.C., et al. "Adaptive neural network sliding mode control of shipboard container cranes considering actuator backlash", *Mechanical systems and signal processing* 112, pp. 233-250. (2018)
[9] Sun, N., Wu, Y., Fang, Y., et al. "Nonlinear antiswing control for crane systems with double-pendulum swing effects and uncertain parameters: Design and experiments", *IEEE Transactions on Automation Science and Engineering* 15(3), pp. 1413-1422. (2017)
[10] Zhang, M., Ma, X., Song, R., et al. "Adaptive proportional-derivative sliding mode control law with improved transient performance for underactuated overhead crane systems", *IEEE/CAA Journal of Automatica Sinica* 5(3), pp. 683-690. (2018)
[11] Alhassan, A.B., Shehu, M.A., Muhammad, B.B., et al. "Sliding Mode Observer-Based Super-Twisting Controller for Under-Actuated Bridge Cranes Subject to Double-Pendulum Effect", *IEEE Access* (2023).
[12] Wang, T., Zhou, J., Zhang, Q., et al. "Design of Adaptive Time-Varying Sliding Mode Controller for Underactuated Overhead Crane Optimized via Improved Honey Badger Algorithm", *Journal of Intelligent & Robotic Systems* 108(3), pp. 39. (2023)
[13] Zhang, M., Zhang, Y., Chen, H., et al. "Model-independent PD-SMC method with payload swing suppression for 3D overhead crane systems", *Mechanical Systems and Signal Processing* 129, pp. 381-393. (2019)
[14] Wang, L., Wu, X., Lei, M., et al. "A new regulation control method for underactuated 3D overhead cranes", *Transactions of the Institute of Measurement and Control* 45(5), pp. 828-837. (2023)
[15] Zhang, S., He, X., Zhu, H., et al. "PID-like coupling control of underactuated overhead cranes with input constraints", *Mechanical Systems and Signal Processing* 178, pp. 109274. (2022)
[16] Miao, X., Zhao, B., Wang, L., et al. "Trolley regulation and swing reduction of underactuated double-pendulum overhead cranes using fuzzy adaptive nonlinear control", *Nonlinear Dynamics* 109(2), pp. 837-847. (2022)
[17] Rigatos, G. "Nonlinear Optimal Control for the Underactuated Double-Pendulum Overhead Crane", *Journal of Vibration Engineering & Technologies*, pp. 1-21. (2023)
[18] Shen, P.Y., Schatz, J. and Caverly, R.J. "Passivity-based adaptive trajectory control of an underactuated 3-DOF overhead crane", *Control Engineering Practice* 112, pp. 104834. (2021)
[19] Zhang, H., Zhao, C. and Ding, J. "Online reinforcement learning with passivity-based stabilizing term for real time overhead crane control without knowledge of the system model", *Control Engineering Practice* 127, pp. 105302. (2022)
[20] Shu, K., Liu, B., Huang, J., et al. "A hierarchical anti-swing control method based on end effector for 2D underactuated overhead cranes system", In *2022 34th Chinese Control and Decision Conference (CCDC)*, pp. 5738-5743. IEEE, (2022).
[21] Bao, H., Kang, Q., An, J., et al. "A performance-driven MPC algorithm for underactuated bridge cranes", *Machines* 9(8), pp. 177. (2021)
[22] Qian, Y., Fang, Y. and Lu, B. "Adaptive robust tracking control for an offshore ship-mounted crane subject to unmatched sea wave disturbances", *Mechanical Systems and Signal Processing* 114, pp. 556-570. (2019)
[23] Rawlings, J.B., Mayne, D.Q. and Diehl, M. “Model predictive control: theory, computation, and design", Vol. 2. Madison, WI: Nob Hill Publishing (2017)
[24] Murray, R.M. “LQR Control”, In *Control and Dynamical Systems.* (2006)
[25] García, L., Barreiro-Gomez, J., Escobar, E., et al. "Modeling and real-time control of urban drainage systems: A review", *Advances in Water Resources* 85, pp. 120-132. (2015)
[26] Impram, S.T., Botto, M.A. and Costa, J. "Robust pole placement controller design for flexible transmission system", *Control and intelligent systems* 32(3), pp. 167-175. (2004)
[27] Michalczuk, M., Ufnalski, B. and Grzesiak, L.M. "Imposing constraints in a full state feedback system using multithreaded controller", *IEEE Transactions on Industrial Electronics*, 68(12), pp.12543-12553. (2020)

10. Captions

Figures

Figure 1: Three-dimensional overhead crane with two inputs and four outputs system dynamics
Figure 2: Displacement (a), Velocity (b), Angle Between Hanging load and Vertical Axis (c) and Angular Velocity Between Hanging load and Vertical Axis (d) Regulation Diagrams along the x-axis (blue line) and y-axis (orange line) by using Pole-Placement in the Alternate System with four inputs
Figure 3: Displacement (a), Velocity (b), Angle Between Hanging load and Vertical Axis (c) and Angular Velocity Between Hanging load and Vertical Axis (d) Regulation Diagrams along the x-axis (blue line) and y-axis (orange line) by using Pole-Placement in the Main System with two inputs
Figure 4: Block Diagram of a System with Pole-Placement Controller [26]
Figure 5: Diagram of the Location of the Trolley (a) and the Fluctuations of the Hanging Load (b) Controlled by Pole-Placement Controller to Reach (3,4) meters Point along the x-axis (blue curve) and y-axis (orange curve)
Figure 6: Diagram of the Input Force to the System Controlled by Pole-Placement Controller to Reach (3,4) meters Point along the x-axis (blue curve) and y-axis (orange curve)
Figure 7: Diagram of the Location of the Trolley (a) and the Fluctuations of the Hanging Load (b) Controlled by Pole-Placement Controller to Reach (0.3,0.4) meters Point along the x-axis (blue curve) and y-axis (orange curve)
Figure 8: Diagram of the Input Force to the System Controlled by Pole-Placement Controller to Reach (0.3,0.4) meters Point along the x-axis (blue curve) and y-axis (orange curve)
Figure 9: Block Diagram of a System with MPC Controller [27]
Figure 10: Diagram of the Location of the Trolley (a), the Fluctuations of the Hanging Load (b), the Input Force (c) to the system Controlled by MPC Controller to Reach (3,4) meters Point along the x-axis (blue curve) and y-axis (orange curve)
Figure 11: Diagram of the Location of the Trolley (a), the Fluctuations of the Hanging Load (b), the Input Force (c) to the system Controlled by MPC Controller to Reach (0.3,0.4) meters Point along the x-axis (blue curve) and y-axis (orange curve)
Figure 12: Comparison between Location considering blue for x-axis and orange for y-axis, dashed line for MPC and straight line for Pole Placement (a), Fluctuations of the Hanging Load along the x-axis (b) and y-axis (c) of the Trolley Controlled by MPC Controller and Pole-Placement Controller for reaching (0.3,0.4) meters point
Figure 13: Comparison between Input Forces of the System Controlled by MPC Controller and Pole-Placement Controller for reaching (0.3,0.4) meters point
Figure 14: Comparison between Location considering blue for x-axis and orange for y-axis, dashed line for MPC and straight line for Pole Placement (a), Fluctuations of the Hanging Load along the x-axis (b) and y-axis (c) of the Trolley Controlled by MPC Controller and Pole-Placement Controller for reaching (3,4) meters point
Figure 15: Comparison between Input Forces of the System Controlled by MPC Controller and Pole-Placement Controller for reaching (3, 4) meters point
Figure 16: Comparison between Location along the x-axis (a) and y-axis (b) of the System Controlled by MPC Controller and Pole-Placement Controller for reaching (0.3, 0.4) meters point with and without 10% of Uncertainties where blue and orange lines indicated MPC and Pole Placement and dashed lines illustrates uncertainties in each of them
Figure 17: Comparison between Fluctuation of the Hanging Load along the x-axis (top) and y-axis (down) of the System controlled by Pole-Placement Controller for reaching (0.3, 0.4) meters point with and without 10% of Uncertainties

Figure 18: Comparison between Fluctuation of the Hanging Load along the x-axis (top) and y-axis (down) of the Main System (blue) and the Uncertain System (orange) controlled by MPC Controller for reaching (0.3, 0.4) meters point with and without 10% of Uncertainties

Tables

Table 1: Detailed information of parameters used in MPC controller

Table 2: Statistical specifications of the main behavior parameters of the system responding to pole-placement controller and MPC

Figures and Tables

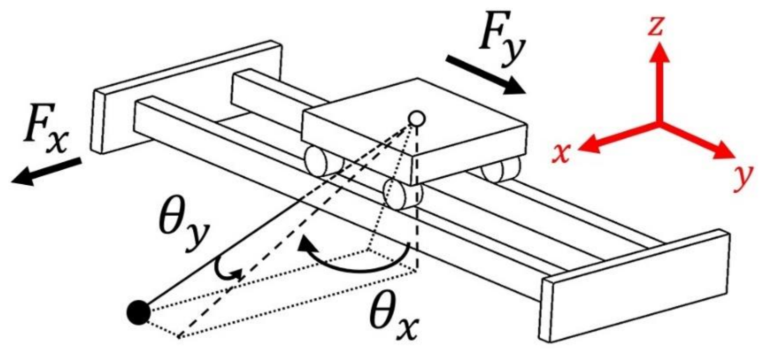

Figure 1

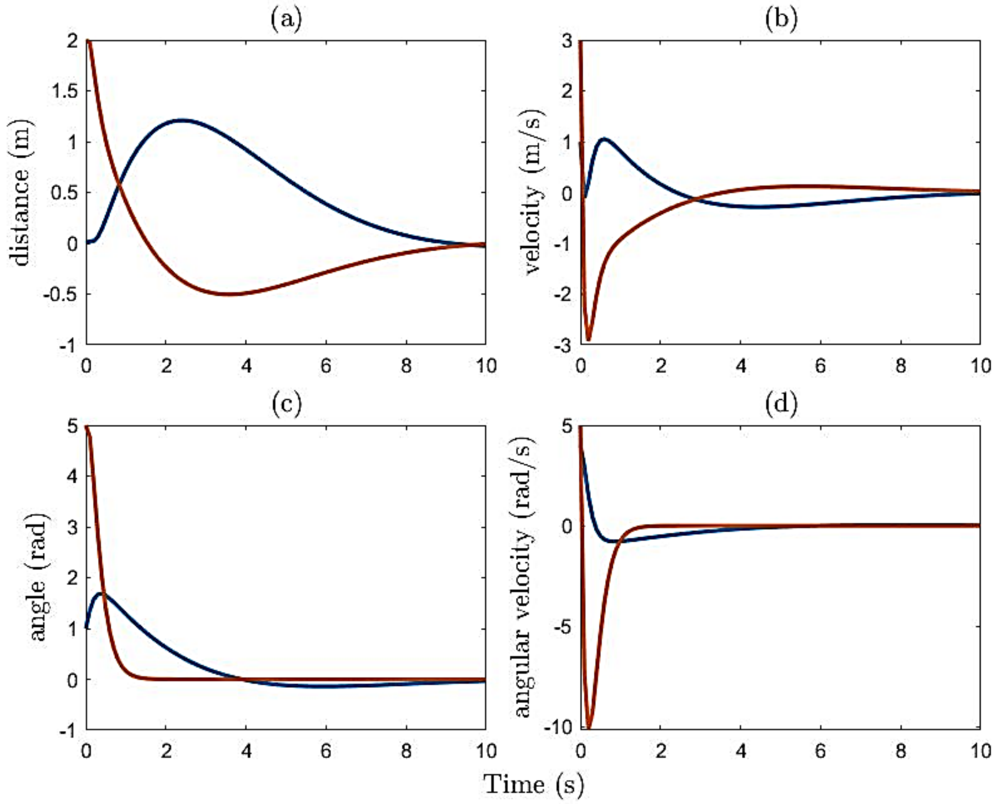

Figure 2

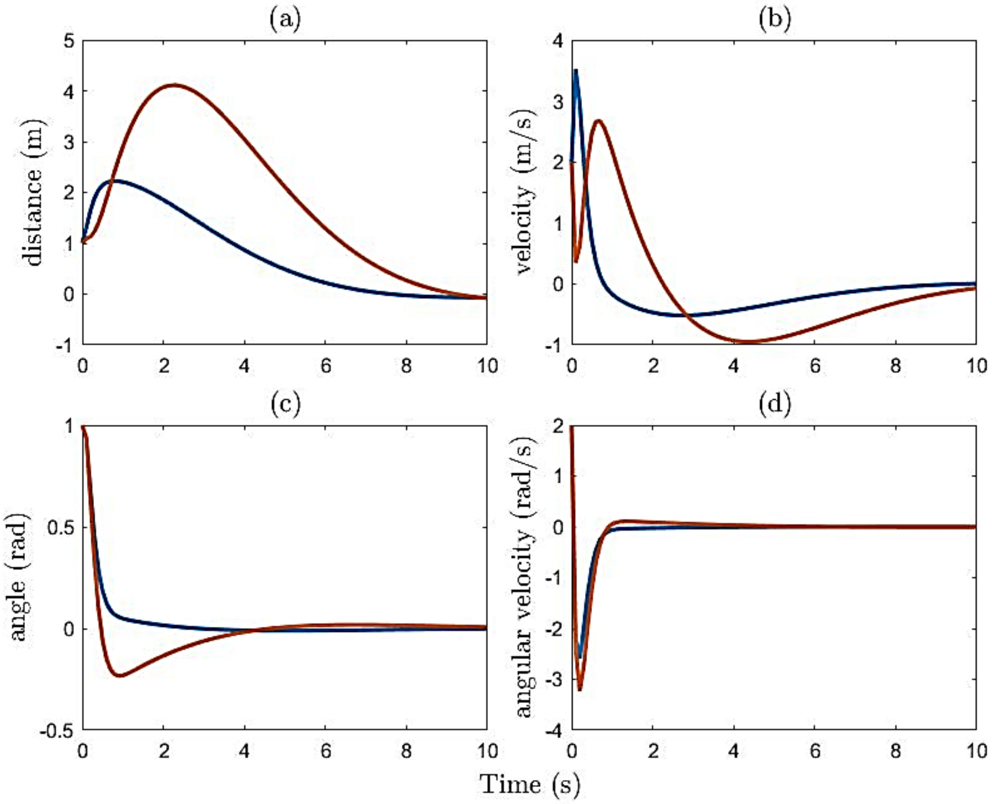

Figure 3

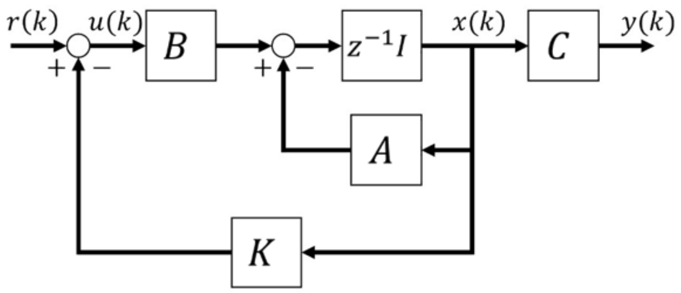

Figure 4

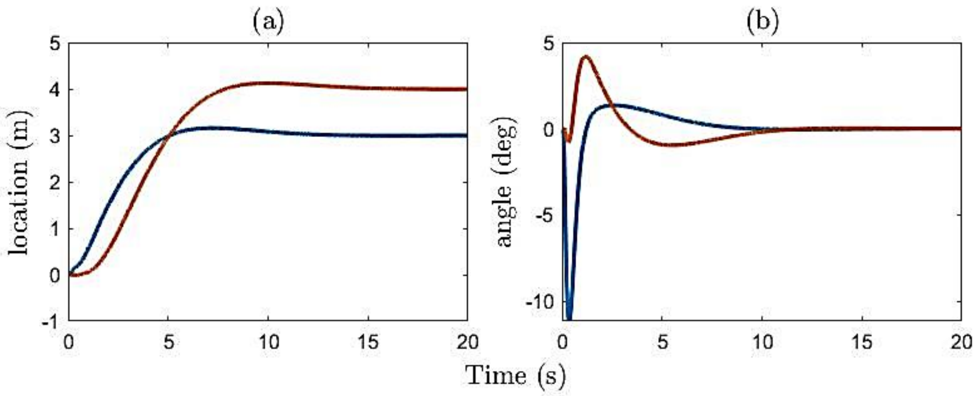

Figure 5

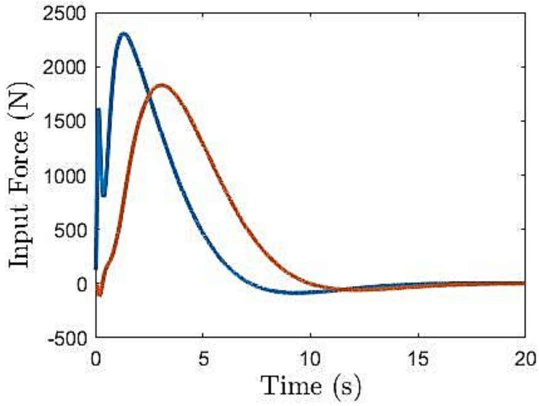

Figure 6

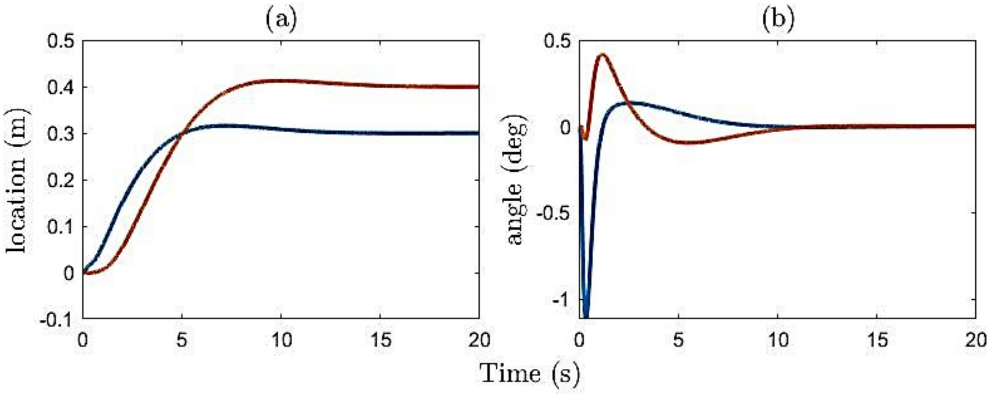

Figure 7

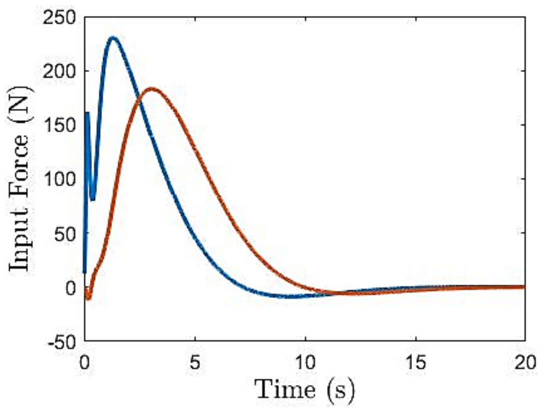

Figure 8

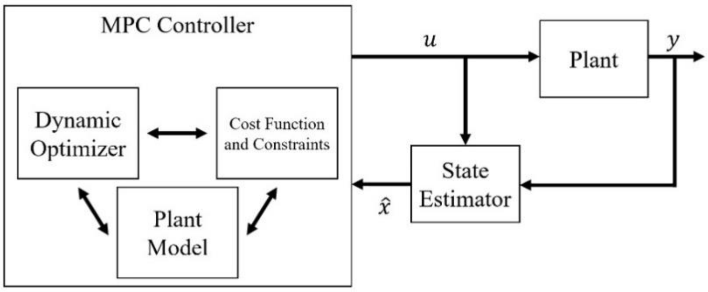

Figure 9

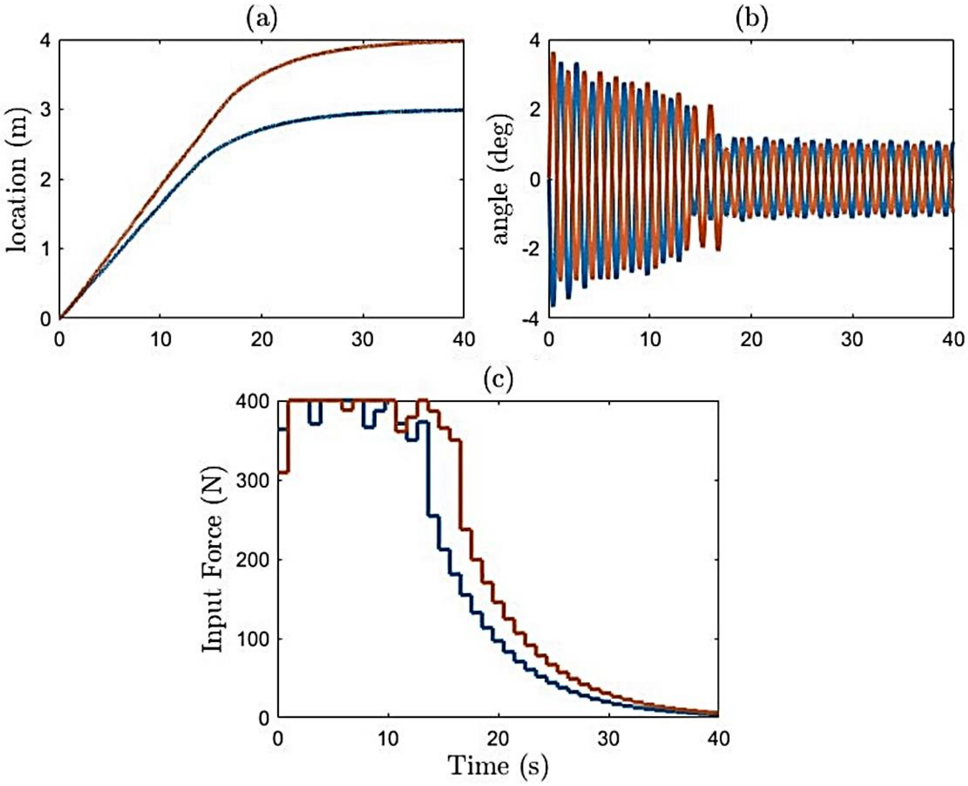

Figure 10

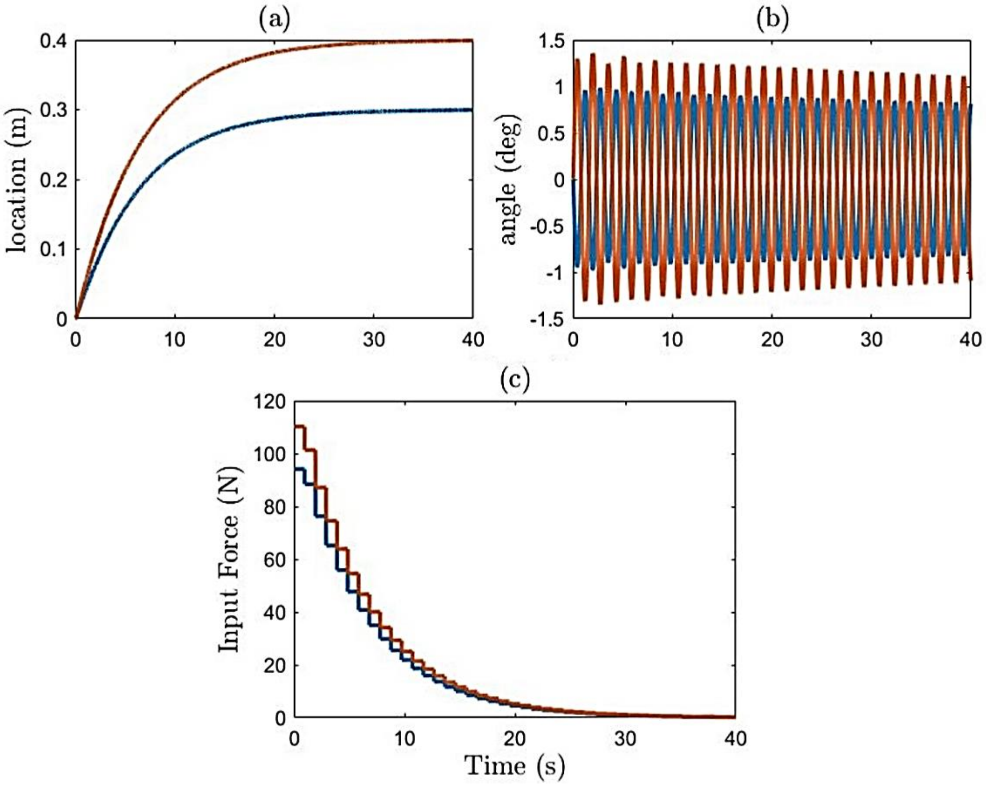

Figure 11

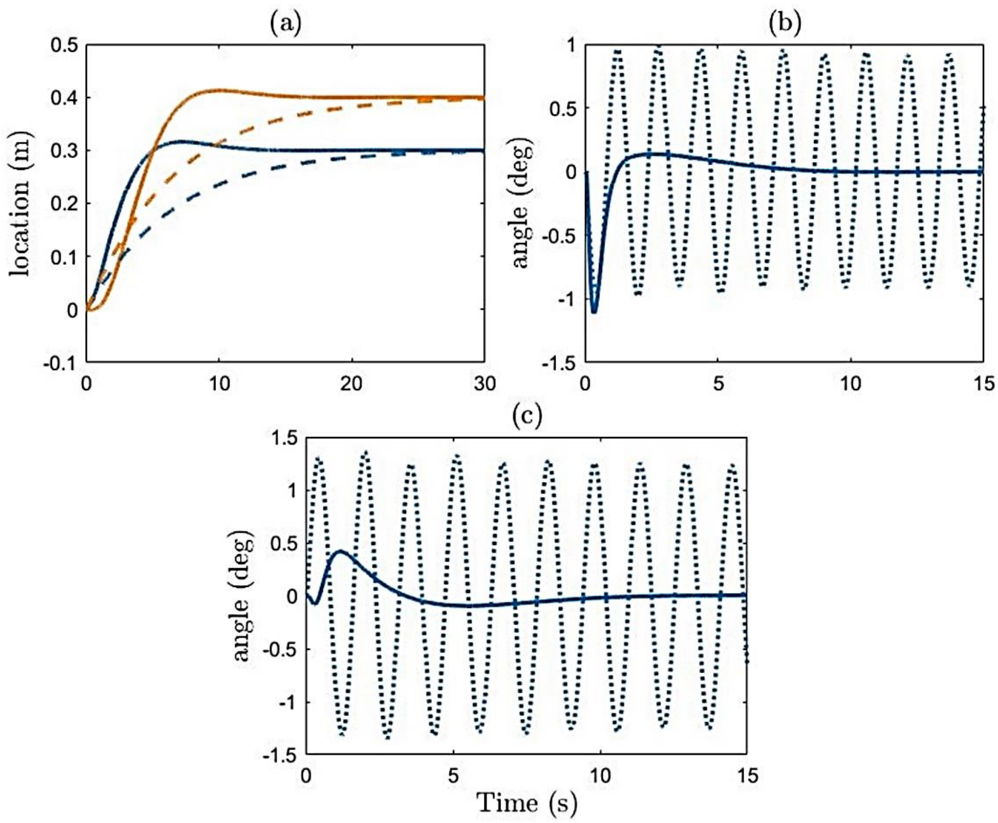

Figure 12

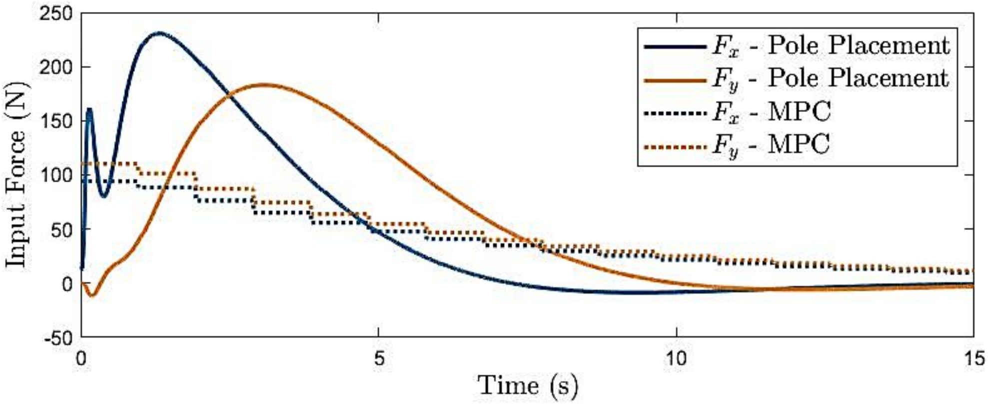

Figure 13

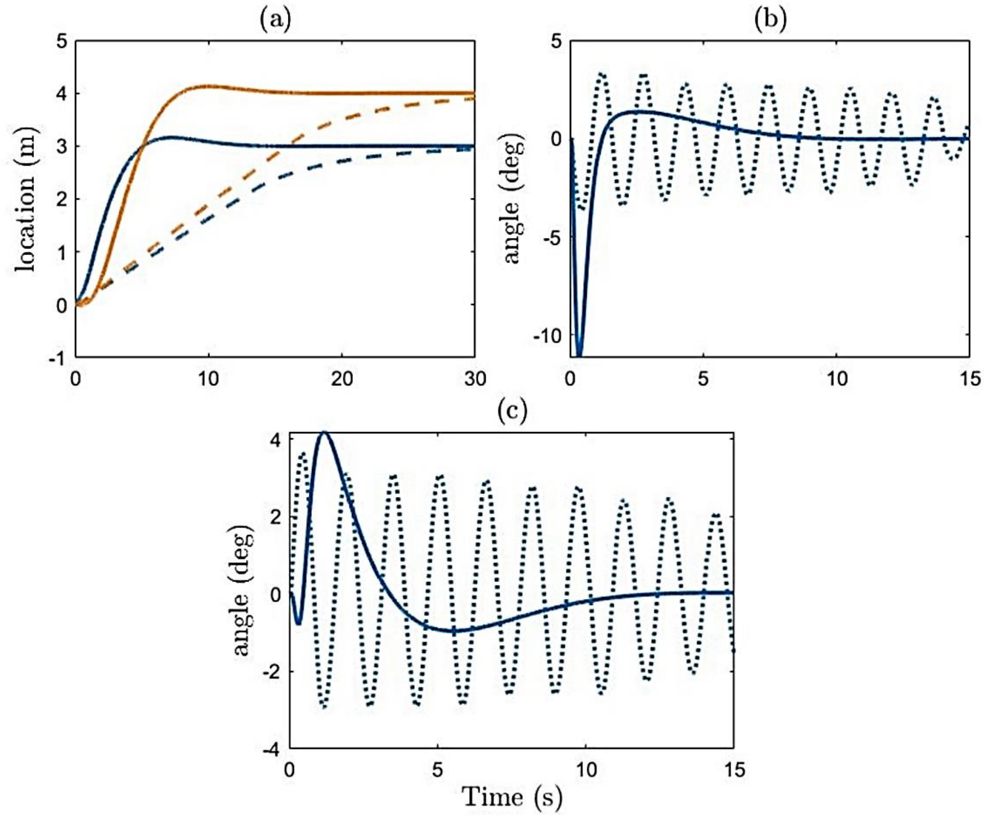

Figure 14

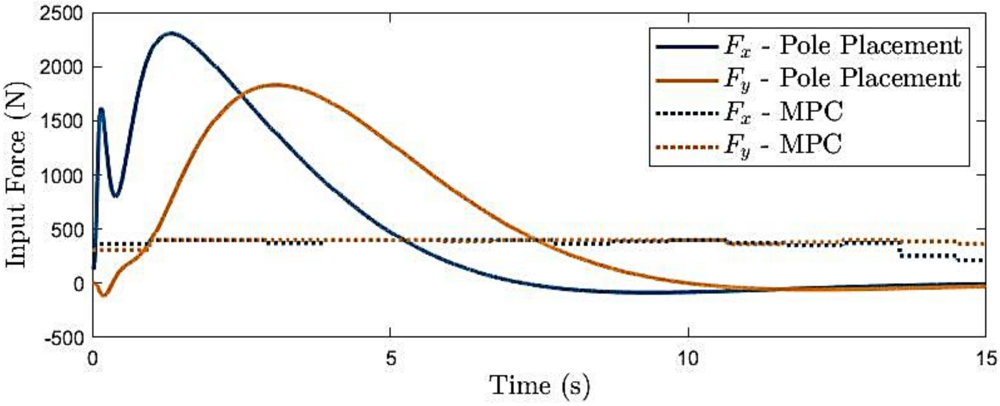

Figure 15

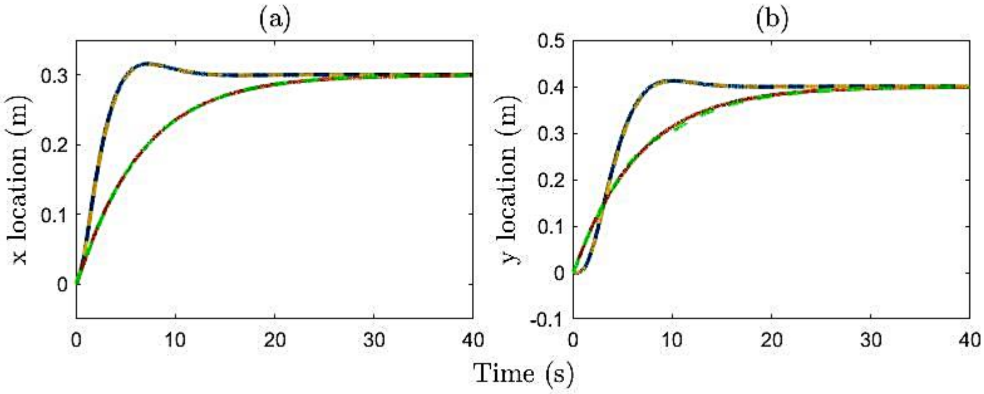

Figure 16

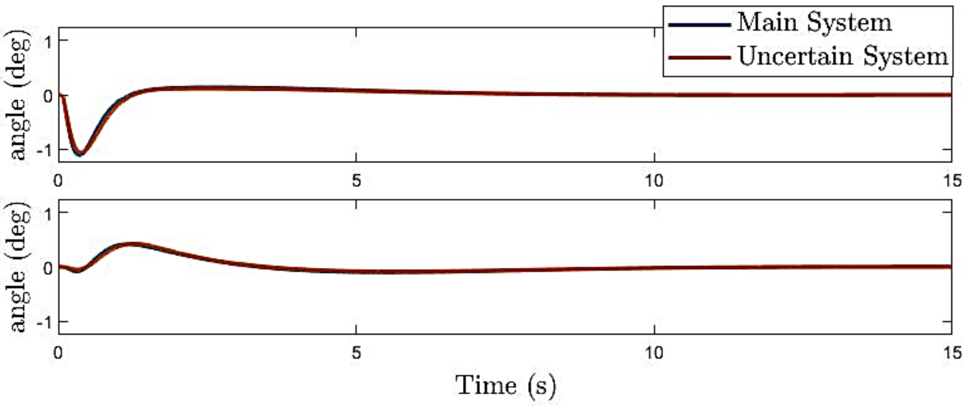

Figure 17

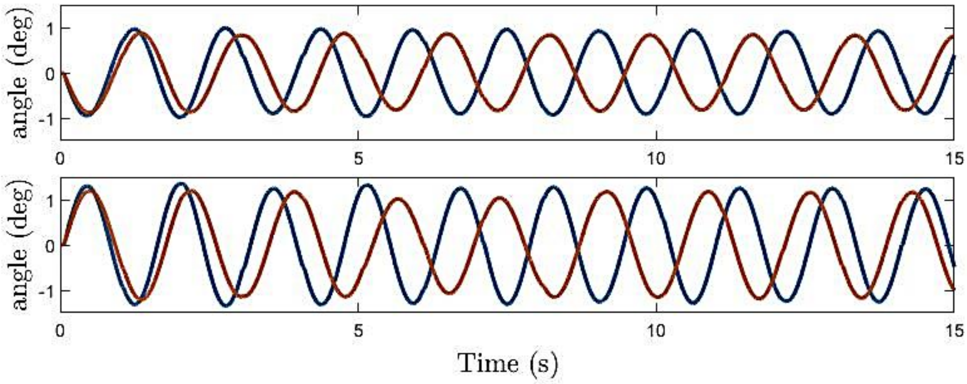

Figure 18

T_s	$1\ s$
p	$10\ s$
m	$1\ s$
x Weight	2
y Weight	2
θ_x Weight	1
θ_y Weight	1
x Constraints	$[-inf, inf]$
y Constraints	$[-inf, inf]$
θ_x Constraints	$[-2^{\circ}, 2^{\circ}]$
θ_y Constraints	$[-2^{\circ}, 2^{\circ}]$
F_x Constraints	$[-inf, 400\,N]$
F_y Constraints	$[-inf, 400\,N]$

Table 1

Controller	Short Trajectory					Long Trajectory				
	Max. Overshoot		Set. Time (s)		Max. Input Force (N)	Max. Overshoot		Set. Time		Max. Input Force (N)
	Avg. Dist.	Avg. Angle	Avg. Dist.	Avg. Angle		Avg. Dist.	Avg. Angle	Avg. Dist.	Avg. Angle	
Pole-Placement	3.75%	10.5°	10	10	225	3.75%	10.5°	10	10	2250
MPC	-	1°	20	15	110	-	3.5°	30	15	400

Table 2

Technical Biography of the Authors

Mohammad Javad Hatami Tajik is currently a MSc student of Mechanical Engineering in the Department of Mechanical Engineering, Sharif University of Technology. His current research interests include the control and automation, system dynamics, non-linear systems and model simulations, application of different type of controllers in systems and designing them, trajectory generation and path control, obstacle avoidance, cable actuators.

Hamed Moradi is currently the Associate Professor in the Department of Mechanical Engineering, Sharif University of Technology. His current research interests include the modeling of dynamic systems, application of robust, nonlinear and optimal control methods in various dynamics systems such as manufacturing, bio-engineering, thermo-fluid industrial processes and power plant engineering. Also, he investigates the analysis of nonlinear dynamics and chaos in various oscillatory phenomena and especially in two areas of thermo-fluid systems and machining chatter vibrations.